

Journal of Biomedical Optics

SPIEDigitalLibrary.org/jbo

Single-camera polarization-sensitive full-field optical coherence tomography with polarization switch

Kwan Seob Park
Woo June Choi
Tae Joong Eom
Byeong Ha Lee

Single-camera polarization-sensitive full-field optical coherence tomography with polarization switch

Kwan Seob Park,^a Woo June Choi,^b Tae Joong Eom,^c and Byeong Ha Lee^a

^aGwangju Institute of Science and Technology, School of Information and Communications, 261 Cheomdan-gwagiro, Buk-gu, Gwangju 500-712, Republic of Korea

^bUniversity of Washington, Department of Bioengineering, 3720 15th Avenue NE, Seattle, Washington 98195

^cGwangju Institute of Science and Technology, Advanced Photonics Research Institute, 261 Cheomdan-gwagiro, Buk-gu, Gwangju 500-712, Republic of Korea

Abstract. We present a single-channel detection-based polarization-sensitive full-field optical coherence tomography (PS-FF-OCT) for simultaneous acquisition of high-resolution OCT and linear retardance images. A linearly polarized sub-10-fs laser was used as a broadband light source for the OCT system. A bi-stable polarization switching device, composed of a ferroelectric liquid crystal cell and an analyzer, was employed to get the horizontal and the vertical polarization components of a full-field interference signal. The time-switched two perpendicular interference signals were sequentially recorded by a single charge-coupled device camera, then processed to extract *en-face* functional images of a biological sample. The rat tail tendon was imaged *ex vivo* to confirm the imaging feasibility of the proposed system, which showed axial and transverse resolutions of 2 and 1.3 μm , respectively. © The Authors. Published by SPIE under a Creative Commons Attribution 3.0 Unported License. Distribution or reproduction of this work in whole or in part requires full attribution of the original publication, including its DOI. [DOI: 10.1117/1.JBO.18.10.100504]

Keywords: polarization sensitive; full-field optical coherence tomography; single-channel detection.

Paper 130566LR received Aug. 6, 2013; revised manuscript received Oct. 8, 2013; accepted for publication Oct. 9, 2013; published online Oct. 28, 2013.

Polarization-sensitive optical coherence tomography (PS-OCT) is a functional extension of OCT and able to produce images of the structural and polarization properties of biological tissue with a micrometer resolution.¹ Phase retardance, being a key feature of PS-OCT and previously providing supplementary tissue information, now offers new insight into the evaluation of tissue inhomogeneity, which has contributed to a broad range of OCT applications including ophthalmology,² dermatology,³ gynecology,⁴ and oncology.⁵ Recent PS-OCT systems have

been based on frequency-domain OCT (FD-OCT) because of the advantages of the high-speed imaging rate⁶ and high sensitivity.⁷ As an alternative to the FD-based PS-OCT, the PS full-field OCT (PS-FF-OCT) has been proposed.⁸ Despite its rather low sensitivity and imaging speed compared with the FD-OCT, the PS-FF-OCT is attractive for its ability to provide images of the functional structure at a subcellular level.

Previous studies on PS-FF-OCT, however, used two identical charge-coupled device (CCD) cameras as detectors to get two perpendicularly polarized interference images. In such a dual-channel detection scheme, precise positioning between the two CCD cameras is imperative so to prevent pixel mismatching between the two CCD images, which causes image deformation. Further, the use of an additional CCD camera also requires added cost and extra space in system implementation. To address these issues, we propose a single-channel detection scheme of PS-FF-OCT. Most of the previously reported single-channel PS-OCTs were based on fiber-scanning OCT techniques,⁹⁻¹² in which a one-dimensional line CCD camera, not a two-dimensional area CCD camera, was used.

To get the full-field interference images in both polarization states with a single CCD camera, a bi-stable polarization switching (BSPS) device was implemented, which consists of a ferroelectric liquid crystal (FLC) cell and a linear polarizer or a polarizing optics.¹³ Typically, the standard FLC cell is fabricated as a half-wave retarder,¹⁴ which causes chromatic or phase errors in broadband applications. However, in our experiment, an achromatic FLC waveplate (Displaytech Inc., Carlsbad, California) was used, which was designed and assembled so that the retardance was a half-wave in the broadband spectral range (~ 300 nm). The achromatic FLC cell works at a center wavelength of 820 nm, which can switch its fast axis in 80 μs and be modulated up to 20 kHz.

A schematic of the experimental setup is shown in Fig. 1. As a broadband light source, a Ti:Sapphire sub-10 femto-pulsed laser (Rainbow, Femtolasers Inc., Viena, Austria) was used in experiments. Spectral bandwidth of the source was 130 nm at full-width half-maximum (FWHM) with an 800-nm center wavelength, and the average output power was approximately 320 mW. An extremely broad bandwidth of the laser was partially cut off from 720 nm, due to the limited spectral responsivity of achromatic quarter wave plates (AQWPs), linear polarizers (LPs), and the FLC cell. We applied a spectral filter to minimize optical aberration, allowing the transmitted spectral bandwidth with 127 nm at FWHM. Accordingly, the axial resolution of the system was calculated to be ~ 1.7 μm in water, but was measured as 2.0 μm experimentally, which was affected by residual dispersion or the non-Gaussian spectral shape of the source spectrum. The output beam from the laser was delivered through a 22-m long multimode fiber (MMF) with a core diameter of 400 μm to reduce spatial coherence within the FF-OCT light source.¹⁵

The beam from the MMF passed through the field stop, aperture stop, and achromatic doublet lens, designed for the Köhler illumination. After that, the beam was split by a beam splitter (BS) into reference and sample arms. Both arms were equipped with identical water immersion microscope objectives and the AQWPs. Also, a neutral density filter for attenuation of light intensity and a glass plate to match the dispersion with the reference arm were positioned in reference and sample arms, respectively. For the sample arm, the AQWP was set to be oriented at 45 deg so that the linearly polarized input beam changes into a

Address all correspondence to: Byeong Ha Lee, Gwangju Institute of Science and Technology, School of Information and Communications, 261 Cheomdan-gwagiro, Buk-gu, Gwangju 500-712, Republic of Korea. Tel: 82-62-715-2234; Fax: 82-62-715-2204; E-mail: leebh@gist.ac.kr; Tae Joong Eom, Gwangju Institute of Science and Technology, Advanced Photonics Research Institute, 261 Cheomdan-gwagiro, Buk-gu, Gwangju 500-712, Republic of Korea. Tel: 82-62-715-3344; Fax: 82-62-715-3419; E-mail: eomtj@gist.ac.kr

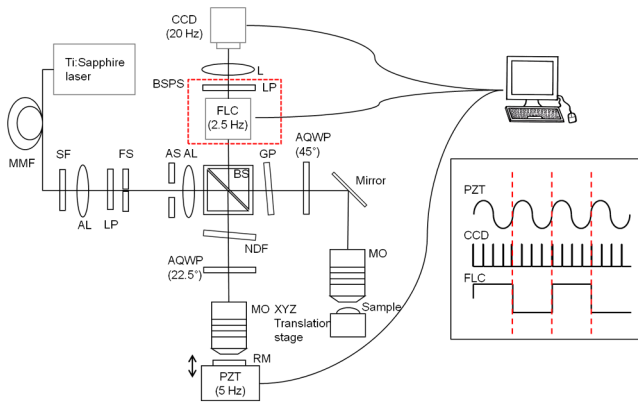


Fig. 1 Schematic of the proposed polarization-sensitive full-field optical coherence tomography (PS-FF-OCT) system: MMF, multimode fiber; SF, spectral filter; AL, achromatic lens; LP, linear polarizer; FS, field stop; AS, aperture stop; NDF, neutral density filter; AQWP, achromatic quarter wave plate; MO, microscope objective; PZT, piezoelectric transducer; RM, reference mirror; GP, glass plate; FLC, ferroelectric liquid crystal cell; CCD, charge coupled device camera. Inset is the timing chart of the PZT, CCD, and FLC cell under synchronization.

circularly polarized one. For the reference arm, the AQWP was set to be oriented at 22.5 deg; the polarization direction of the round trip beam was oriented at 45 deg, and vertical and horizontal polarization components of the round trip beam thus had identical amounts. The beams reflected and backscattered from the reference and the sample arms recombined at the BS. The combined beams passed through the BS device and then were detected by the single CCD camera (CCD1020, 10-bits, 512x512 pixels, 20 frames/s, VDS).

As depicted in the inset of Fig. 1, the piezoelectric transducer (PZT), the CCD camera, and the FLC cell were synchronized to each other and operated at 5, 20, and 2.5 Hz, respectively. A set of four CCD frames ($E_1^\perp, E_2^\perp, E_3^\perp, E_4^\perp$) were captured during one period of PZT under sinusoidal phase modulation to capture the vertical component of the interfered beam. The consecutive set of four CCD frames ($E_5^\parallel, E_6^\parallel, E_7^\parallel, E_8^\parallel$) were taken during the next period of the PZT modulation to provide the horizontal component of the interfered beam. Finally, intensity and phase retardation images were calculated from measured vertical and horizontal polarization components as explained in Ref. 8. Those can be expressed as $\Gamma^\perp = (E_1^\perp - E_2^\perp)^2 + (E_3^\perp - E_4^\perp)^2$ and $\Gamma^\parallel = (E_5^\parallel - E_6^\parallel)^2 + (E_7^\parallel - E_8^\parallel)^2$. The retardation image could be constructed by taking the ratio of Γ^\parallel and Γ^\perp . The intensity image was also made by the summation of Γ^\parallel and Γ^\perp at the same time.

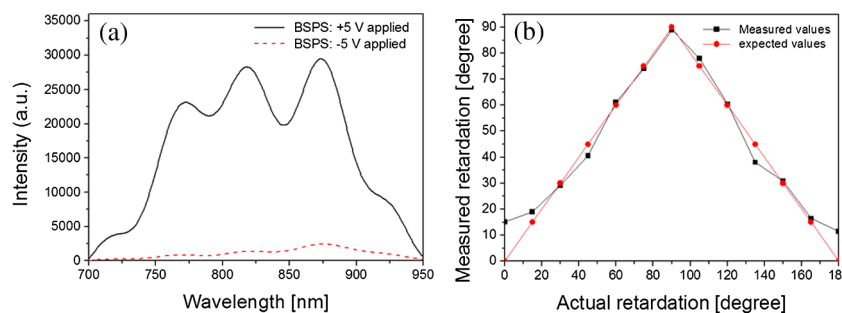


Fig. 2 (a) Spectral performance of the bi-stable polarization switching (BSPS) device at an applied voltage of +5 and -5 V. (b) Measured retardation in relation to actual retardation using the Babinet compensator.

To validate the system performance, we measured the transmission spectrum after passing through the BS and measured the retardation using the proposed FF-PS-OCT system with a sample of known retardation state. Figure 2(a) shows the wavelength dependency of the BS with the switching signals. The vertically polarized light was passing through the BS device, while the transmission axis of the linear polarizer was installed in the vertical direction. The transmission was suppressed around -11 dB at -5 V switching signal.

The Babinet compensator was used to generate a certain birefringence-induced phase retardation to the system and placed between the BS and the microscope objective (MO) in the sample arm. To match the dispersion with the sample arm, a glass plate of appropriate thickness corresponding to the compensator was positioned in the reference arm. While rotating the graduations on the compensator by the amount giving 15-deg phase retardation, phase retardation values were measured. Every measurement was carried out by averaging 10 frames. The measured retardation was plotted with given retardation, as shown in Fig. 2(b). The polarization-induced phase retardation was linearly increased with the actual retardation, but it showed relatively high errors around the zero retardation. This discrepancy between expected and measured retardations can be caused by the remaining transmission light from the low-extinction ratio of the FLC cell.

To confirm the performance of the system in the given biological tissue, a rat tail tendon was prepared and imaged with water immersion micro-objectives (Olympus, 10x, NA 0.3, MO), which gives a theoretical spatial resolution of $\sim 1.3 \mu\text{m}$. The skin of the rat tail was peeled by a stripper so to view and image the tendon directly. During the experiment, the prepared rat tail tendon was immersed in phosphate-buffered saline to maintain a constant pH in the biological tissue immersion medium. To prevent CCD camera image saturation, the launched power was heavily attenuated by a linear polarizer and an attenuator. The illumination power on the sample was about $25 \mu\text{W}$. The acquisition time for one PS-FF-OCT image took approximately 0.4 s, and 10 images were averaged for one depth-resolved image.

Figure 3 shows PS-FF-OCT images of the rat's tail tendon with its polarization-induced phase retardation images. Several strands of tendon with crimp patterns adjoin each other, as shown in Fig. 3(a). Secondary fiber bundles (fascicles) and even subfascicles (digits 1 to 4) of the tendon, which are invisible with conventional PS-OCT in general, are clearly visible in the XY and YZ images, respectively. Figure 3(b) shows the linear retardance image taken at the same depth of the intensity image of Fig. 3(a). The phase retardation from 0 to 90 deg

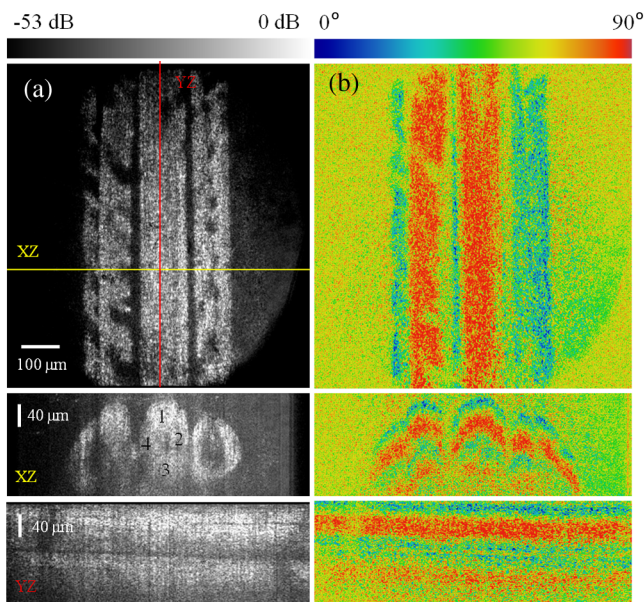


Fig. 3 *Ex vivo* images of the rat tail tendon by PS-FF-OCT: (a) *En-face* intensity images at a depth of $43\ \mu\text{m}$; XZ and YZ cross-sectional images. (b) *En-face* retardation image at the same depth with (a); XZ and YZ cross-sectional retardation images.

was expressed with pseudo-color mapping. The cross-sectional image shows the variation of phase retardation along and across the tendons.

In summary, we have constructed a single-channel PS-FF-OCT using a BSPS device, which consists of a FLC cell and an LP. The BSPS device was positioned in front of the CCD camera to rotate the polarization state of the scattered light, providing a geometric separation of two perpendicular components of interfered light. As a result, the temporal split of two polarization components enabled a single CCD camera to collect two polarization components. Thanks to the high-resolution nature of PS-FF-OCT, the fascicle structure of the tendon was apparent with its retardation image. This method provides a simple process and relatively easy alignment of the PS-FF-OCT system.

Acknowledgments

This research was partially supported by the National Research Foundation of Korea (NRF) grant and funded by the Korea government (MSIP) (No. 2008-0062606, CELA-NCRC, 2010-0024058) and the Industrial Strategic Technology

Development Program funded by the Ministry of Trade, Industry & Energy, Republic of Korea (10040121). We are grateful to Prof. Euiheon Jung of department of medical engineering for providing rat's tail tendon as an imaging sample.

References

1. D. Huang et al., "Optical coherence tomography," *Science* **254**(5035), 1178–1181 (1991).
2. B. Cense et al., "In vivo depth-resolved birefringence measurements of the human retinal nerve fiber layer by polarization-sensitive optical coherence tomography," *Opt. Lett.* **27**(18), 1610–1612 (2002).
3. J. F. de Boer et al., "Imaging thermally damaged tissue by polarization sensitive optical coherence tomography," *Opt. Express* **3**(6), 212–218 (1998).
4. S.-W. Lee et al., "Optical diagnosis of cervical intraepithelial neoplasm (CIN) using polarization-sensitive optical coherence tomography," *Opt. Express* **16**(4), 2709–2719 (2008).
5. K. H. Kim et al., "Polarization-sensitive optical frequency domain imaging based on unpolarized light," *Opt. Express* **19**(2), 552–561 (2011).
6. M. Bonesi et al., "High-speed polarization sensitive optical coherence tomography scan engine based on Fourier domain mode locked laser," *Biomed. Opt. Express* **3**(11), 2987–3000 (2012).
7. B. Baumann et al., "Swept source/Fourier domain polarization sensitive optical coherence tomography with a passive polarization delay unit," *Opt. Express* **20**(9), 10229–10241 (2012).
8. G. Moneron, A.-C. Boccara, and A. Dubois, "Polarization-sensitive full-field optical coherence tomography," *Opt. Lett.* **32**(14), 2058–2060 (2007).
9. T. Schmoll et al., "Single-camera polarization-sensitive spectral-domain OCT by spatial frequency encoding," *Opt. Lett.* **35**(2), 241–243 (2010).
10. W. Y. Oh et al., "Single-detector polarization-sensitive optical frequency domain imaging using high-speed intra A-line polarization modulation," *Opt. Lett.* **33**(12), 1330–1332 (2008).
11. M. Zhao and J. A. Izatt, "single-camera sequential-scan-based polarization-sensitive SDOCT for retinal imaging," *Opt. Lett.* **34**(2), 205–207 (2009).
12. S.-W. Lee, H.-W. Jeong, and B.-M. Kim, "High-speed spectral domain polarization-sensitive optical coherence tomography using a single camera and an optical switch at $1.3\ \mu\text{m}$," *J. Biomed. Opt.* **15**(1), 010501 (2010).
13. V. Toubaev et al., "Quasi-holographic solution to polarization-sensitive optical coherence tomography acceptable to nonlaboratory applications," *J. Biomed. Opt.* **13**(4), 044014 (2008).
14. M. O. Freeman, T. A. Brown, and D. M. Walba, "Quantized complex ferroelectric liquid crystal spatial light modulators," *Appl. Opt.* **31**(20), 3917–3929 (1992).
15. W. J. Choi et al., "Tomographic imaging of a suspending single live cell using optical tweezer-combined full-field optical coherence tomography," *Opt. Lett.* **37**(14), 2784–2786 (2012).